



A. Chatterjee,<sup>1,2</sup> A. Navin,<sup>1,\*</sup> A. Shrivastava,<sup>2</sup> S. Bhattacharyya,<sup>1</sup> M. Rejmund,<sup>1</sup> N. Keeley,<sup>3,4</sup> V. Nanal,<sup>9</sup>  
 J. Nyberg,<sup>6</sup> R.G. Pillay,<sup>5</sup> K. Ramachandran,<sup>2</sup> I. Stefan,<sup>1</sup> D. Bazin,<sup>7</sup> D. Beaumel,<sup>8</sup> Y. Blumenfeld,<sup>8</sup> G. de France,<sup>1</sup>  
 D. Gupta,<sup>8</sup> M. Labiche,<sup>9</sup> A. Lemasson,<sup>1</sup> R. Lemmon,<sup>9</sup> R. Raabe,<sup>1</sup> J.A. Scarpaci,<sup>8</sup> C. Simenel,<sup>3</sup> and C. Timis<sup>10</sup>

<sup>1</sup>GANIL, CEA/DSM - CNRS/IN2P3, Bd Henri Becquerel, BP 55027, F-14076 Caen Cedex 5, France

<sup>2</sup>Nuclear Physics Division, Bhabha Atomic Research Centre, Mumbai 400085, India

<sup>3</sup>DSM/IRFU/SPhN, CEA Saclay, F-91191 Gif sur Yvette, France

<sup>4</sup>Department of Nuclear Reactions, The Andrzej Soltan Institute for Nuclear Studies, Hoza 69, PL-00-681 Warsaw, Poland

<sup>5</sup>DNAP, Tata Institute of Fundamental research, Mumbai 400005, India

<sup>6</sup>Department of Physics and Astronomy, Uppsala University, Uppsala, Sweden

<sup>7</sup>National Superconducting Cyclotron Laboratory, Michigan State University, East Lansing, Michigan, 48824, USA

<sup>8</sup>Institut de Physique Nucléaire, IN2P3-CNRS, 91406 Orsay, France

<sup>9</sup>CRLC, Daresbury Laboratory, Daresbury, Warrington, WA4 4AD, U.K.

<sup>10</sup>Department of Physics, University of Surrey, Guildford, GU2 7XH, U.K.

Angular distributions for 1n- and 2n-transfer are reported for the  ${}^6\text{He} + {}^{65}\text{Cu}$  system at  $E_{lab} = 22.6$  MeV. For the first time, triple coincidences between  $\alpha$  particles, neutrons and characteristic  $\gamma$  rays from the target-like residues were used to separate the contributions arising from 1n- and 2n-transfer. The differential cross sections for these channels, elastic scattering, and fusion were analyzed using a Coupled Reaction Channels approach. The large measured ratio of the 2n/1n cross section and the strong influence of 2n-transfer on other channels indicate that the di-neutron configuration of  ${}^6\text{He}$  plays a dominant role in the reaction mechanism.

PACS numbers: 25.60.-t, 24.50.+g, 25.70.Jj

Reactions near the Coulomb barrier have been shown to be an ideal tool to study the effect of multidimensional tunneling and obtain information about the structure of the interacting nuclei [1]. New features arising from the weak binding in nuclei far from stability in reactions near the Coulomb barrier have been recently discussed [2]. Neutron-rich nuclei near the drip line, especially Borromean nuclei, offer a unique environment to study neutron correlations at low densities, which are necessary inputs for nuclear structure models and the study of neutron stars. Theoretical analyses suggest that at low neutron density strong spatial di-neutron correlations are expected [3, 4]. Such correlations have been theoretically studied in two-neutron Borromean nuclei like  ${}^6\text{He}$  and  ${}^{11}\text{Li}$  [5]. The structure of the lightest two-neutron halo nucleus,  ${}^6\text{He}$ , with an inert  $\alpha$  core and known  $\alpha$ -n interaction has been investigated via a variety of techniques [6–9], mainly at energies well above the Coulomb barrier.

The 2n/1n transfer cross section ratio can provide information about the structural correlation of neutrons in  ${}^6\text{He}$ . The cigar shape, where the two neutrons lie on opposite sides of the  $\alpha$  particle, should preferentially populate  ${}^5\text{He}$  by 1n-transfer while the di-neutron configuration should be responsible mainly for 2n-transfer [10]. The recently reported charge radii of  ${}^6,8\text{He}$  provide an independent method of studying correlations in these Borromean nuclei [11]. Michel *et al.* have investigated the Wigner threshold law in weakly-bound nuclei using the Gamow shell model [12], showing the influence of the Wigner cusp on the spectroscopic factors. Thus, the study of transfer angular distributions with Borromean nuclei is of interest in the context of this general phe-

nomenon observed in various fields of physics [13].

Measurements of  $\alpha$ -n coincidences in the  ${}^6\text{He} + {}^{209}\text{Bi}$  system at an energy of 22 MeV showed the relative dominance of the 2n channel [14, 15]. Reactions on medium-mass targets are experimentally more challenging and are also controversial with respect to the influence of weak binding on the fusion process [16]. Theoretical treatment of reactions involving Borromean projectiles, especially at near-barrier energies, is a complex problem as calculations have to include the unbound spectrum of a four-body system. However, state-of-the-art continuum discretized coupled-channel calculations taking into account the three-body nature of  ${}^6\text{He}$  [17, 18] or its simplification as a 2n+ $\alpha$  cluster [19] have been performed. These calculations can presently compute only elastic scattering and breakup; a theoretical formalism able to describe simultaneously elastic scattering, transfer and breakup is desirable but not yet available.

With the motivation of understanding the Borromean structure and its influence on reactions around the Coulomb barrier, we report a novel triple coincidence measurement of angular distributions of transfer channels with an ISOL beam. A first theoretical attempt, for Borromean nuclei, towards understanding the importance of coupling to transfer channels for elastic scattering and fusion is also presented.

An intense ( $\sim 4 \times 10^7$  pps)  ${}^6\text{He}$  beam at an energy of 22.6 MeV was obtained from the ISOL facility SPIRAL at GANIL. The target was a 2.6 mg/cm<sup>2</sup> thick self supporting  ${}^{65}\text{Cu}$  foil, isotopically enriched to 99.7%. Beam intensities were measured with a high stability current amplifier connected to a Faraday cup. The detec-

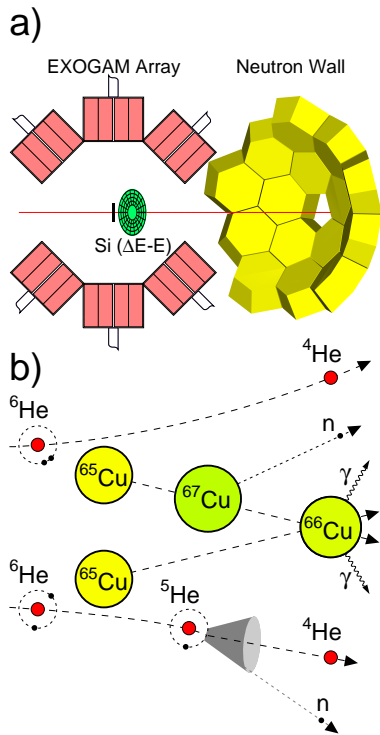


FIG. 1: (color online) Schematic of (a) The experimental setup. (b) Reaction mechanism for  $2n$ - and  $1n$ -transfer

tion setup (Fig. 1a) consisted of an annular Si telescope, the EXOGAM  $\gamma$  array [20] with 11 Compton-suppressed clovers, and a neutron array of 45 liquid scintillator elements [21].

Charged particles were detected and identified in an annular Si telescope comprising  $\Delta E$  ( $\sim 50 \mu\text{m}$ ) and  $E$  ( $\sim 500 \mu\text{m}$ ) elements with active inner and outer diameters of 22 mm and 70 mm covering an angular range of  $\sim 25^\circ$  to  $60^\circ$  at 2.5 cm from the target. The angular resolution was  $\simeq 1.7^\circ$ . The solid angles of each ring/sector combination were determined both by simulations and comparison with elastic scattering measurements on a Au target. The energy resolution for elastically scattered particles was  $\simeq 300 \text{ keV}$ . The neutron wall consisted of 45 hexagonal detectors at 55 cm from the target, covering  $\simeq 18\%$  of  $4\pi$  [21]. The time of flight (TOF) was obtained with respect to the  $E$  detector of the annular telescope with a resolution of  $\simeq 3 \text{ ns}$  (corresponding to an energy resolution of  $270 \text{ keV}$  at  $E_n=1.5 \text{ MeV}$ ). Neutrons were separated from  $\gamma$  rays by two-dimensional gates in the TOF vs. pulse-shape discrimination plot and detected at mean angles of  $19^\circ$ ,  $30^\circ$ ,  $35^\circ$ ,  $47^\circ$ , and  $57^\circ$  with an angular resolution of  $\pm 6.5^\circ$ . Small corrections for cross talk between the neutron detectors were included [22]. Absolute efficiencies of the neutron detectors as a function of energy were determined from a comparison of the measured neutron spectra from a  ${}^{252}\text{Cf}$  source placed at the target position and the known multiplicity and spec-

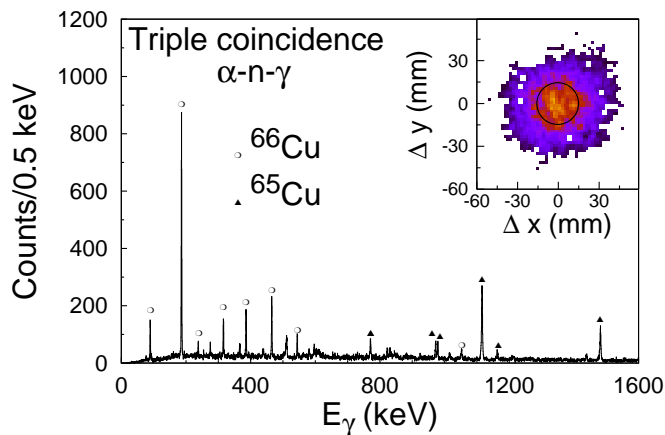


FIG. 2: (color online) Gamma spectrum in coincidence with  $\alpha$  particles and neutrons obtained by selecting events outside the region marked in the inset (see text). The inset shows a 2D plot of the difference in positions of the detected  $\alpha$  particle and neutron at the plane of the Si detector.

tral shape [23]. The measured efficiencies compared well with Monte Carlo simulations of the neutron array [22]. Eleven Compton-suppressed clover detectors at 14.7 cm from the target were used to select the residual nuclei by a measurement of their characteristic  $\gamma$  rays. Cross sections for the evaporation residue channels were obtained from characteristic  $\gamma$  ray yields, following the method of Ref. [16]. The total fusion cross section was obtained from the sum of the measured evaporation residue cross sections. Statistical model calculations using the code CASCADE [24] showed good agreement for all residues except  ${}^{66}\text{Cu}$ . The yield of  ${}^{66}\text{Cu}$  from fusion evaporation is negligible ( $\approx 5\%$ ); it is produced mainly by  $1n$ - and  $2n$ -transfer (see also [16]).

Fig. 1b gives a schematic of the reaction mechanism, indicating that due to the Borromean nature of  ${}^6\text{He}$  the final state is similar in both  $1n$ - and  $2n$ -transfer. In both cases we have a neutron, an  $\alpha$  particle and  $\gamma$  rays from the excited  ${}^{66}\text{Cu}$  residue. Transfer is a selective process, peaking for a narrow window of matching conditions in the angular and linear momenta of the particles. In the present case,  $2n$ -transfer leads to the formation of  ${}^{67}\text{Cu}$  with an excitation energy sufficient to evaporate one neutron (isotropically), while  $1n$ -transfer leads to states in  ${}^{66}\text{Cu}$  which decay by  $\gamma$  emission. Hence there is a kinematic correlation (conditions on energies and emission angles) between  $\alpha$  particles and neutrons for  $1n$ -transfer but not for  $2n$ -transfer. Triple coincidences between  $n$ ,  $\alpha$  and  $\gamma$  rays from the excited  ${}^{66}\text{Cu}$  residue were used to deconvolute the  $1n$ - and  $2n$ -transfer contributions and eliminate projectile breakup. Extraction of the transfer cross section was as follows. Events with conditions for neutron,  $\alpha$  particle and  $\gamma$  transitions in  ${}^{66}\text{Cu}$  were first selected. These were then used to obtain the angles and energies of the selected neutrons and  $\alpha$  particles and their

relative angles  $\theta_{n\alpha}$  and energies  $E_{n\alpha}$ . Population of the  $3/2^-$  ground state of  ${}^5\text{He}$  was verified from the measured correlation between  $\theta_{n\alpha}$  and  $E_{n\alpha}$ . For  $1n$ -transfer, neutrons and  $\alpha$  particles are emitted by the breakup of  ${}^5\text{He}$  in this state. Reaction kinematics restricts  $\theta_{n\alpha}$  to a maximum value ( $\theta_0$ ) of  $31^\circ$  for these events. Such a directional correlation is absent in the case of  $2n$ -transfer where the neutron arises by evaporation from excited  ${}^{67}\text{Cu}$  nuclei (see Fig. 1b). Thus the region  $\theta_{n\alpha} > \theta_0$  consists of events arising from  $2n$ -transfer and the corresponding differential cross sections were obtained by restricting to events in this region. The region  $\theta_{n\alpha} < \theta_0$  contains contributions from both  $2n$ - and  $1n$ -transfer. Fig. 2 shows the sum of the added-back  $\gamma$ -ray spectrum in coincidence with  $\alpha$  particles and neutrons for  $\theta_{n\alpha} > \theta_0$ . Prominent transitions in  ${}^{66}\text{Cu}$  and those in  ${}^{65}\text{Cu}$  (arising from the  $\alpha 2n$  fusion-evaporation channel) are indicated. The inset shows the division of the kinematic region in a two-dimensional plot of  $\Delta x$  vs.  $\Delta y$ , where  $\Delta x$  and  $\Delta y$  are the differences in position of the detected  $\alpha$  particle and neutron at the plane of the Si detector. The central region (marked by a circle in the inset) represents the  $31^\circ$  cone. Differential cross sections for  $1n$ -transfer were obtained by subtracting the  $2n$ -transfer contribution obtained from the yields outside the cone (scaled with the appropriate solid angles) from the total yields in this region. The emission angle of  ${}^5\text{He}$  was approximated as the measured  $\theta_\alpha$ . The fraction of the solid angle of the neutron wall corresponding to the two regions, inside and outside the cone, was obtained from simulations.

Absolute cross sections were obtained from the known efficiencies, target thickness and integrated beam intensity. Angular distributions for  $1n$ - and  $2n$ -transfer are plotted in Fig. 3a; only statistical errors are shown, ranging from 2-3 % and 15-20 % for the  $2n$  and  $1n$ -transfer, respectively. For  $1n$ -transfer  $\theta_{{}^5\text{He}}$  was assumed to be equal to  $\theta_\alpha$ . The relative insensitivity of the extracted cross sections to the precise value of  $\theta_0$  was verified by repeating the analysis with a  $5^\circ$  variation. The elastic scattering angular distribution is shown in Fig. 3b.

Coupled Reaction Channel (CRC) calculations [2] were performed using the code FRESKO [25] to understand the angular distributions and the role of channel coupling in the various processes. The full complex remnant term and non-orthogonality correction were included. Coupling to breakup channels was not considered, based on a lower breakup contribution (as compared to transfer) observed in [26] and the reduced importance of Coulomb breakup for this lower  $Z$  target. Entrance and exit channel potentials consisted of double-folded real and interior Woods-Saxon imaginary parts. The M3Y effective interaction [27] and  ${}^6\text{He}$  and  ${}^5\text{He}$  matter densities from Refs. [28] and [29], respectively were used to calculate the real potential. The Woods-Saxon potential parameters were:  $W = 50$  MeV,  $R = 1.0 \times (A_p^{1/3} + A_t^{1/3})$  fm,  $a = 0.3$  fm.

The positive  $Q$ -value of the  ${}^{65}\text{Cu}({}^6\text{He}, {}^5\text{He}){}^{66}\text{Cu}$  re-

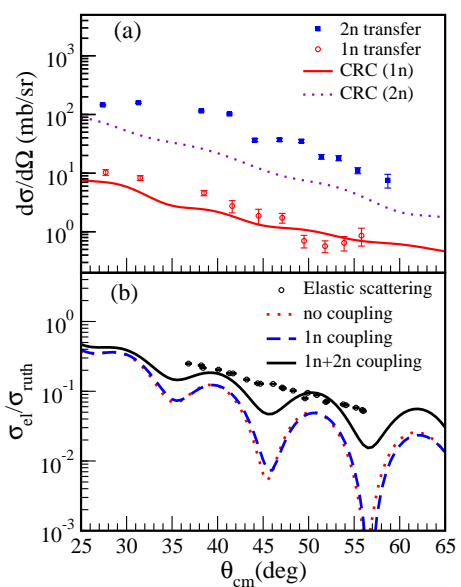


FIG. 3: (color online) Angular distributions for  ${}^6\text{He} + {}^{65}\text{Cu}$ . (a)  $1n$ - and  $2n$ -transfer; calculations for  $1n$  and  $2n$ -transfer are shown. (b) Elastic scattering; calculations with no coupling (dotted curve),  $1n$ -transfer couplings only (dashed line) and both  $1n$ - and  $2n$ -transfer couplings (solid line) are shown.

action favors population of relatively high-lying states. However, the  $(2J+1)S$  values derived from an analysis of the  ${}^{65}\text{Cu}(d,p)$  reaction show a rather rapid decrease with increasing excitation energy (below  $\sim 3$  MeV) [30]. Thus, a limited number of states in  ${}^{66}\text{Cu}$  were included. Configurations, spectroscopic factors and  $n+{}^{65}\text{Cu}$  potentials were from Refs. [30, 31]. Transfer to the  $3/2^-$  resonance of  ${}^5\text{He}$  only was included, with spectroscopic factor from Ref. [32] and Woods-Saxon  $n+{}^5\text{He}$  potential with radius parameter  $r_0 = 1.25$  fm, diffuseness  $a = 0.65$  fm, and a spin-orbit component of the same geometry and a depth of 6 MeV.

Inclusion of  $2n$ -transfer in the calculation is more challenging, the  $Q$ -value for this reaction favoring high-lying states in  ${}^{67}\text{Cu}$ . The  $Q$ -matching condition, together with the fact that no  $\gamma$  rays for transitions in  ${}^{67}\text{Cu}$  were observed, suggests that if the mechanism is conventional transfer only states above the  $1n$  separation threshold in  ${}^{67}\text{Cu}$  (9.1 MeV) but below the  $2n$  threshold (16.2 MeV) should be considered. Two-step sequential transfer was omitted, as attempting to include it would increase the number of unknowns in the calculation. Due to the lack of information on high-lying states in  ${}^{67}\text{Cu}$  we extrapolated the similarity of the low-lying spectra of  ${}^{65}\text{Cu}$  and  ${}^{67}\text{Cu}$  observed in  $(p,t)$  reactions [33] to higher excitation energies. Transfer to states in  ${}^{67}\text{Cu}$  from 10.9 to 14.3 MeV, with spins, parities and excitation energies of known states in  ${}^{65}\text{Cu}$  [34] was included. A di-neutron-like cluster structure for these states with the lowest possible

$2n$  angular momentum relative to the  $^{65}\text{Cu}$  was assumed. The  $2n+^{65}\text{Cu}$  potentials were of Woods-Saxon form, radius  $R = 1.25 \times (2^{1/3} + 65^{1/3})$  fm and diffuseness  $a = 0.65$  fm; all spectroscopic factors were set to 1.0. The form factor for the  $2n+^4\text{He}$  overlap of  $^6\text{He}$  was from Ref. [35]. The optical potential was the same double-folded plus Woods-Saxon combination as in the other channels, with  $^4\text{He}$  matter density derived from the charge density [36].

Calculated angular distributions for transfer and elastic scattering are shown in Fig. 3. The solid curve in Fig. 3a is the sum of the angular distributions for  $1n$ -transfer to individual states in  $^{66}\text{Cu}$ ; the agreement with data is good, supporting the assumption that the mechanism is conventional single-neutron stripping to bound states in  $^{66}\text{Cu}$ . The  $2n$ -transfer result, denoted by the dotted line in Fig. 3a, reproduces well the shape of the angular distribution; the difference in absolute magnitude is not surprising in view of the uncertainties in the  $2n$ -transfer calculation. These results support the suggestion, prompted by the very large cross section, that the  $2n$ -transfer is largely the result of a direct, one-step transfer of a di-neutron-like cluster.

The effect of transfer couplings on the elastic scattering is shown in Fig. 3b; the dotted curve denotes the no-coupling calculation and the dashed curve the effect of coupling to  $1n$ -transfer only. It can be seen that this coupling has a small effect. The solid curve denotes the result of the calculation including both  $1n$ - and  $2n$ -transfer couplings. The effect of coupling to the  $2n$ -transfer channel is much stronger than that of  $1n$ -transfer, acting to further damp the oscillations and increase the larger angle cross section to better match the data. Although the elastic scattering is still oscillatory compared to the data, a problem usually associated with insufficient absorption, the magnitude is well described. The fusion cross section was calculated using the in-going wave boundary condition. Calculations with no coupling, coupling to  $1n$ -transfer only and to both  $1n$ - and  $2n$ -transfer give values of 1655, 1631 and 1551 mb, respectively, in good agreement with the measured fusion cross section of 1396(90) mb. The influence of  $1n$ -transfer coupling on total fusion, like that on the elastic channel, is weak. The relatively good agreement between the measured and calculated values for the various channels in this system seen in Fig. 3 represents an important step towards an understanding of the reaction mechanism for Borromean nuclei at near-barrier energies. Earlier work [15] pointed out the large  $\alpha$ -particle yield in reactions involving  $^6\text{He}$ . In particular, the results with a  $^{209}\text{Bi}$  target find a ratio of  $2n$ - to  $1n$ -transfer cross section of about 2.5-3. For the medium mass target studied here this ratio is about 10; the difference could be due to the role of target structure.

In summary, exclusive measurements of  $1n$ - and  $2n$ -transfer, elastic scattering and fusion for the Borromean nucleus  $^6\text{He}$  incident on a medium mass target at an energy near the Coulomb barrier are reported. The first

successful application for a low-energy ISOL beam of triple coincidences between  $\alpha$ -, neutrons and  $\gamma$  rays from the target-like residue and their angular correlations was used to obtain uniquely the  $1n$ - and  $2n$ -transfer angular distributions. The present work shows that the main contribution to transfer is due to the  $2n$  component, thereby indicating [10] the dominance of the di-neutron structure in  $^6\text{He}$ . CRC calculations illustrate the important role played by coupling to the two neutron channel in the reaction mechanism. The availability of low energy beams of double Borromean  $^8\text{He}$ , having the highest N/Z ratio, would provide an excellent opportunity to study correlations between the four valence neutrons and to investigate the effect of the continuum in this drip line nucleus.

N.K. acknowledges the receipt of a Marie Curie Actions Grant, Contract No. MEIF-CT-2005-010158.

---

\* corresponding author: navin@ganil.fr

- [1] M. Dasgupta *et al.*, Ann. Rev. Nucl. Part. Sci. 48, 401 (1998).
- [2] N. Keeley *et al.*, Prog. Part. Phys. 59, 579 (2007).
- [3] F. Barranco *et al.*, Eur. Phys. J. A 11, 385 (2001); E. Vigezzi *et al.*, Nucl. Phys. A 752, 600 (2005).
- [4] Masayuki Matsuo, Phys. Rev. C 73, 044309 (2006).
- [5] M.V. Zhukov *et al.*, Phys. Rep. 23, 1151 (1993).
- [6] T. Aumann, Eur. Phys. J. A 26, 441 (2005).
- [7] G. M. Ter-Akopian, *et al.*, Phys. Lett. B426, 251 (1998).
- [8] Yu. Ts. Oganessian *et al.*, Phys. Rev. Lett. 82, 4996 (1999).
- [9] M. Marques *et al.*, Phys. Lett. B476, 219 (2000).
- [10] L.I. Galanina *et al.*, Phys. At. Nucl. 70, 283 (2007).
- [11] P. Mueller *et al.*, Phys. Rev. Lett. 99, 252501 (2007).
- [12] N. Michel *et al.*, Phys. Rev. C 75, 031301(R) (2007).
- [13] R.K. Adair, Phys. Rev. 111, 632 (1958).
- [14] J.P. Bychowski *et al.*, Phys. Lett. B596, 26 (2004).
- [15] P.A. DeYoung *et al.*, Phys. Rev. C 71, 051601(R) (2005).
- [16] A. Navin *et al.*, Phys. Rev. C 70, 044601 (2004).
- [17] T. Matsumoto *et al.*, Phys. Rev. C 73, 051602(R) (2006).
- [18] M. Rodriguez-Gallardo *et al.*, Phys. Rev. C 72, 024007 (2005).
- [19] A.M. Moro *et al.*, Phys. Rev. C 75, 064607 (2007).
- [20] J. Simpson *et al.*, Heavy Ion Phys. 11, 159 (2000).
- [21] O. Skeppsted *et al.*, Nucl. Inst. Meth A 421, 531 (1999).
- [22] J. Ljungvall *et al.*, Nucl. Inst. Meth A 528, 741 (2004).
- [23] J.W. Meadows, Phys. Rev. 157, 1076 (1967).
- [24] F. Puhlhofer, Nucl. Phys. A 280, 267 (1977).
- [25] I.J. Thompson, Comp. Phys. Rep. 7, 167 (1988).
- [26] J.J. Kolata *et al.*, Phys. Rev. C 75, 031302(R) (2007).
- [27] G.R. Satchler and W.G. Love, Phys. Rep. 55, 183 (1979).
- [28] J. S. Al-Khalili *et al.*, Phys. Rev. C 54, 1843 (1996).
- [29] T. Neff and H. Feldmeier, Nucl. Phys. A 738, 357 (2004).
- [30] W.W. Daehnick, Y.S. Park, Phys. Rev. 180, 1062 (1969).
- [31] M.R. Bhat, Nucl. Data Sheets 83, 789 (1998).
- [32] O.F. Nemets *et al.*, Nucleon clusters in atomic nuclei and many-nucleon transfer reactions, Ukrainian Academy of Sciences, Institute for Nuclear Research, Kiev, 1988.
- [33] J.H. Bjerregaard *et al.*, Nucl. Phys. 85, 593 (1966).
- [34] M.R. Bhat, Nucl. Data Sheets 69, 209 (1993).

- [35] L. Giot *et al.*, Phys. Rev. C 71, 064311 (2005).  
[36] J.S. McCarthy *et al.*, Phys. Rev. C 15, 1396 (1977).